

8.10 BENCHMARKING IN-FLIGHT ICING DETECTION PRODUCTS FOR FUTURE UPGRADES

M. K. Politovich¹, P. Minnis², D. B. Johnson¹, C. A. Wolff¹, M. Chapman¹, P. W. Heck², and J. A. Haggerty¹

¹ National Center for Atmospheric Research, Boulder, CO

² NASA Langley Research Center, Hampton, VA

1. INTRODUCTION

This paper summarizes the results of a benchmarking exercise conducted as part of the NASA supported Advanced Satellite Aviation-Weather Products (ASAP) Program. The goal of ASAP is to increase and optimize the use of satellite data sets within the existing FAA Aviation Weather Research Program (AWRP) Product Development Team (PDT) structure and to transfer advanced satellite expertise to the PDTs. Currently, ASAP fosters collaborative efforts between NASA Laboratories, the University of Wisconsin Cooperative Institute for Meteorological Satellite Studies (UW-CIMSS), the University of Alabama in Huntsville (UAH), and the AWRP PDTs. This collaboration involves the testing and evaluation of existing satellite algorithms developed or proposed by AWRP teams, the introduction of new techniques and data sets to the PDTs from the satellite community, and enhanced access to new satellite data sets available through CIMSS and NASA Langley Research Center for evaluation and testing.

The In-Flight Icing PDT (IFIPDT) developed the Current Icing Potential (CIP) product, which is now run operationally at the National Weather Service's Aviation Weather Center. This product combines model output with observational data to provide an hourly, three-dimensional, gridded depiction of icing potential. While CIP incorporates GOES information it does so in a relatively rudimentary manner as a cloud mask. For the IFIPDT, the CIP is a natural target for enhancement using advanced satellite products, such as those being developed at NASA's Langley Research Center (LaRC). We anticipate that the accuracy of the CIP should improve as it is extended to include cloud top phase, effective particle size and other attributes of icing severity.

IFIPDT members have already been examining the NASA advanced satellite products during forecasting exercises conducted in support of field research projects conducted during the past two winter seasons. Anecdotally, the forecasters have found these products to be highly useful for flight planning and directing icing flight missions by helping to pinpoint the locations of icing conditions. It is now time to provide quantitative information on the accuracy of the products.

In this paper we begin a process of benchmarking some of the advanced satellite products from LaRC, through comparison with CIP and with PIREPs. In a broader sense, this paper also begins an examination of possible verification methods and strategies appropriate for new products that incorporate high resolution satellite imagery.

2. NASA LANGLEY SATELLITE ICING AND CLOUD PRODUCTS

The Langley cloud products (Minnis et al. 2001) are derived from half-hourly Geostationary Operational Environmental Satellite (GOES) data taken from GOES-10 (West) and GOES-12 (East) using the Visible Infrared Solar-infrared Split-window Technique (VISST) during the daytime (Minnis et al. 1995, 1998). Each 4-km GOES pixel is first classified as clear or cloudy using a complex cloud identification scheme (Trepte et al. 1999). Each of the cloudy pixels is analyzed with the VISST to determine cloud phase, optical depth, effective particle size, effective temperature, effective height, and ice or liquid water path. These parameters are used to estimate cloud-top and base altitudes and temperatures. The analyses utilize the 0.65, 3.9, 10.8, and the 12 or 13 μm GOES imager channels.

A prototype diagnostic aircraft icing index termed "risk factor" (Minnis et al. 2003, 2004) has already been developed through diagnostic comparisons of the Langley cloud products with pilot icing reports (Smith et al. 2000, 2002, 2003). Critical observations include the cloud top temperature T_c , cloud optical depth τ , cloud phase, cloud droplet effective radius r_e , as well as the liquid water path, LWP. The prototype criteria are summarized in Table 1. The logic tree first checks whether the pixel is clear or not. If clear, it is eliminated from further consideration. If cloudy, it will still be eliminated from further processing if the $T_c > 272$ K (too warm for icing), or if it is classified as an ice cloud with $\tau < 8$. This latter criterion is based on an expectation that the optical depth would be larger than this if a significant water cloud were to exist beneath the ice cloud. Any residual water below the ice cloud is not likely to be able to product significant icing. The remaining pixels are then examined further to evaluate their potential to cause icing.

If the observed cloud is classified as ice and has a large optical depth ($\tau > 8$), it is recognized that there is a possibility that a significant water cloud exists within or below the ice cloud, but this can not be resolved by the satellite observations alone. The pixel is therefore

Corresponding author address: M.K. Politovich,
NCAR, P.O. Box 3000, Boulder, CO 80307;
marcia@ucar.edu

classified as unknown or indeterminate. It will require further study or combination with the other CIP data to arrive at a firmer classification. The remaining pixels are all classified as supercooled water clouds. They are classified as having no, low, middle, or high icing potential based on the values of r_e , T_c , and LWP as described in Table 1. Any supercooled water cloud pixels having characteristics that do not satisfy any of the criteria 2 - 9 in Table 1 are not considered to be icing threats.

Table 1: Prototype icing classification criteria for NASA LaRC satellite-based products.

Value	Criterion	Icing Intensity		
0	clear or water cloud	none		
	w/ $T_c > 272$ K			
	or LWP $< 100 \text{ gm}^{-2}$			
	or ice cloud with $\tau < 8$)			
1	ice cloud with $\tau > 8$	unknown		
	r_e (μm)	LWP (gm^{-2})	T_c (K)	
2	> 10	> 100	< 272	low
3	> 10	> 200	< 272	mid
4	> 10	> 300	< 272	high
5	> 8	> 400	< 272	low
6	> 8	> 500	< 272	mid
7	> 10	> 300	< 253	high
8	> 8	> 400	< 253	high

An example of the icing product is shown in Figure 1. Areas with icing potential are apparent over Iowa, western Tennessee, northern North Dakota, around North Carolina, and in the Pacific Northwest. Extensive regions of high cloud cover create a number of areas of "indeterminate" icing. Small areas with potential icing are identified around the edges of some cirrus clouds due to overlapping conditions and edge effects.

As an initial efforts in our benchmarking process we will examine some of the component fields that are used in the LaRC icing classification scheme, starting with the derived cloud phase field. The usefulness of the cloud phase field will be evaluated through a systematic and extensive set of comparisons to PIREPs obtained during 2003 and 2004, and to the current CIP. The systematic approach making use of all

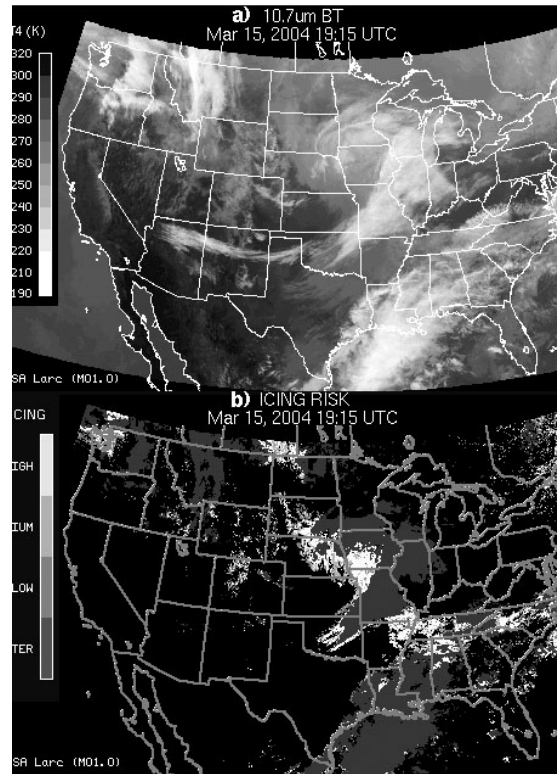


Figure 1. Cloud and icing data for 1915 UTC, 15 March 2004: (a) Stitched GOES-10/12 infrared brightness temperature, (b) Icing categories.

available PIREPs is designed to get beyond qualitative tests that look for patterns that seem realistic and emphasize anecdotal examples of PIREPs in key areas.

3. THE CURRENT ICING POTENTIAL (CIP) PRODUCT

The first In-Flight Icing PDT product to be transferred to operational use in the National Weather Service was the Current Icing Potential (CIP, McDonough et al., 2000 and Bernstein et al. 2004). The CIP algorithm applies fuzzy logic techniques to combine up to fifty-six interest fields into one fused product. CIP combines data from five sources—multispectral GOES imagery, model output from the RUC model, surface observations, NEXRAD radar data, and pilot reports -- and is available on the Aviation Digital Data Service (ADDS) web page at:

<http://adds.aviationweather.noaa.gov>

Figure 2 shows an example of CIP hourly output, with the letters shown on the figure representing the icing type, as reported in a PIREP. The size of the letters is related to the reported icing severity. While CIP icing potential values are usually reported as decimal values between 0 and 1, the color coded scale for this chart is presented as icing potential x 100.

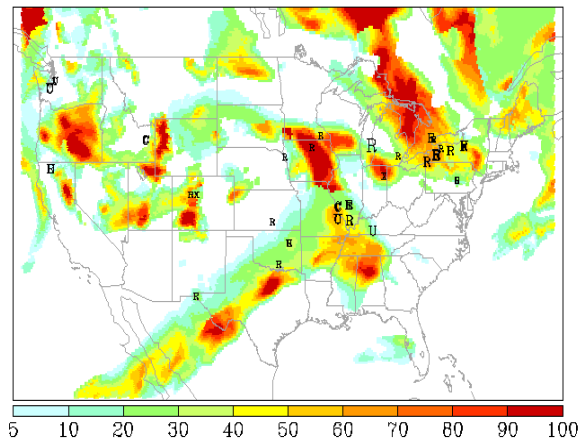


Figure 2: Example of CIP hourly output. This example shows the maximum icing potential value in any 20-km gridded RUC column, for 1800 UTC, 14 Nov. 2003. R=rime; C=clear; X=mixed and U=unknown ice type.

3.1 Verification Methods

The CIP verification was accomplished by evaluating the icing potential field versus pilot reports (PIREPs) of positive and negative icing. Each PIREP was matched to the closest CIP grid point and flight level. The four grid points surrounding the observation, as well as 1,000-ft¹ flight levels above and below the PIREP, were examined. Currently, CIP incorporates information from PIREPs in the hour prior to the forecast time. This analysis therefore only used observations (PIREPs) in a time window of one hour following the forecast valid time. Statistics were then computed and analyzed. The verification statistics for CIP were then compared to the Airmen's Meteorological Advisories (AIRMETs). Although the AIRMETs are generally different than CIP (e.g., they cover a relatively broad volume and are intended to depict icing over a six hour period), the comparison is included because AIRMETs are a readily available operational icing forecast produced by forecasters at the Aviation Weather Center (AWC).

The verification methods utilized in the evaluation of CIP are based on standard verification concepts that recognize the underlying framework for forecast verification and the associated high dimensionality of the verification problem. The methods used are described in greater detail in Brown (1996). The specific icing forecast verification methodology outlined by Brown et al. (1997) treats icing forecasts and observations as YES/NO values. Brown et al. (1999) outline how this method can be extended to forecasts with values on a continuous scale. Specifically, icing

¹ Note that CIP outputs altitudes in ft rather than meters, since these are the units used by the aviation end-users. We will retain these units in this paper rather than converting to metric.

diagnoses produced by CIP can be converted to a set of YES/NO values by applying a variety of thresholds. For example, applying a threshold of 0.30 to CIP diagnoses would lead to a YES value for all grid points with an icing potential value greater than or equal to 0.30 while each grid point with a value less than 0.30 would be assigned a NO value. The verification methods are based on a standard YES/NO two-by-two contingency table (Table 2). Each cell in this table contains a count of the number of times a particular forecast and observation pair was observed. The counts on this table are observation-based (i.e., the sum of the counts is the total number of YES and NO PIREPs over the given time period) and therefore not all CIP grid points are represented.

Table 2: Contingency table for evaluation of dichotomous (e.g., Yes/No) forecasts. The elements in the cells are the counts of forecast-observation pairs.

Forecast	Observations		Total
	Yes	No	
Yes	YY	YN	YY+YN
No	NY	NN	NY+NN
Total	YY+NY	YN+NN	YY+YN+NY+NN

POD_y and POD_n are the primary verification statistics that are included in this evaluation. They are estimates of the proportions of Yes and No observations that are correctly diagnosed. Together, POD_y and POD_n measure the ability of the diagnoses to discriminate between Yes and No icing observations. Table 3 gives the definition and description of these statistics.

Table 3: Verification Statistics used in evaluation of CIP.

Statistic	Definition	Description
POD _y	YY/(YY+NY)	Probability of detection of "YES" observations
POD _n	NN/(YN+NN)	Probability of Detection of "No" observations
TSS	POD _y + POD _n - 1	Level of discrimination between YES and NO observations

The relationship between PODy and 1-PODn for different thresholds is the basis for the verification approach known as “Signal Detection Theory” (SDT). This relationship can be represented for a given algorithm with the curve joining the (1-PODn, PODy) points for different thresholds. The resulting curve is known as the Relative Operating Characteristic (ROC) curve in SDT. The closer this curve comes to the upper left corner, the better the diagnosis. The area under the curve is a measure of overall forecast skill and provides another measure that can be compared among forecast products. This measure is not dependent on the threshold used. A forecast with zero skill would have an ROC area of 0.5 or less.

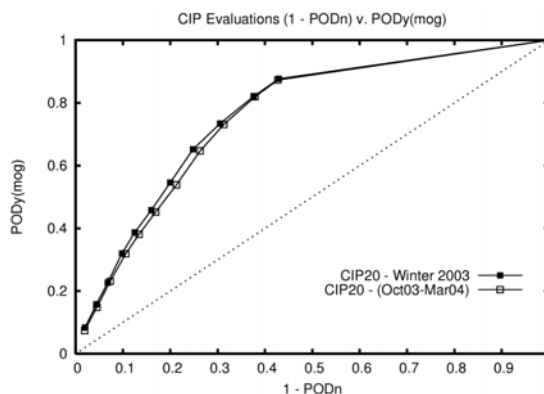


Figure 3: Comparison of PODy(mog) vs. 1-PODn for CIP over winter 2003 and for times valid for Benchmarking period (Oct'03 – Mar'04).

3.2 CIP Data Used for Benchmark Verification

The valid time period for this evaluation was 1 October 2003 to 31 March 2004. The 1500 UTC and 2100 UTC valid times were compared; a total of 341 CIP files were available for verification. All available AIRMETS valid for the specific CIP times were incorporated. The total number of PIREPs used as observations in the evaluation of CIP and the AIRMETS is listed in Table 4.

Table 4: Icing observations included in the CIP verification

Observation	Number of pilot reports
NO	8346
YES (MOG)	1767

3.3 Results

CIP is relatively efficient at detecting icing conditions of detection for MOG YES reports [PODy(MOG) of 0.74-0.82, see Figure 3], and a corresponding probability of detection of NO reports (PODn) between 0.62-0.68, depending on the CIP threshold used. AIRMETS detected a similar number of YES reports with a [PODy(MOG)] of 0.751 also capturing a similar number of NO reports with a PODn of 0.635. For the CIP evaluation, the eleven thresholds used were 0.00, 0.05, 0.15, 0.25, 0.35, 0.45, 0.55, 0.65, 0.75, 0.85, and 0.95. For CIP, the icing potential field is thresholded. For each available PIREP four CIP grid points are compared with 64 GDCP cloud phase pixels. Figure 4 is a ROC plot of all of the CIP thresholds for all of the valid times with the statistics for the AIRMET overlaid. It is a sufficient depiction of how skillful the CIP icing potential field is compared AIRMETS.

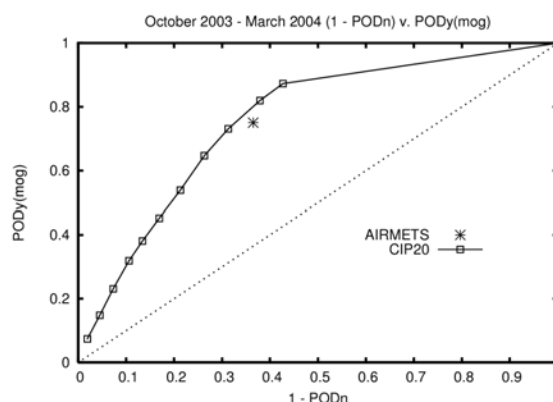


Figure 4: Same as Figure 3, except for CIP and AIRMETS.

4. NASA LaRC GOES-DERIVED CLOUD PRODUCTS (GDCP) VERIFICATION

The GDCP produces several products. The reason that we began these benchmarking studies with the cloud phase product is its direct and obvious correlation to the CIP icing potential. If the phase of the cloud diagnosed at any given pixel is liquid with temperature below 0 °C, one can assume that there is potential for icing because of the presence of supercooled liquid water (SLW).

The verification study for the GDCP is done using PIREPs of positive and negative icing and is very similar to the CIP verification. Although the verification methods are essentially the same, some changes are inevitable because of the differences in the products. CIP is a three-dimensional product, able to be matched to any PIREP in its domain; the GDCP are two-dimensional and can only be considered valid near cloud top. Further, the GDCP also have a finer horizontal resolution than CIP.

4.1 Methods

To ensure a fair verification using established techniques the products must first be put on the same grid. The CIP is run on the 20-km Rapid Update Cycle (RUC) model grid. The GDCP, derived from GOES pixels with a nominal 4-5 km resolution, have been remapped to a RUC projection, but with a 5-km grid. To ensure that the higher resolution satellite products are not penalized for their increased horizontal resolution, the analysis has to be extended to cover the same special domain as used in the CIP verification already discussed. In the CIP study, each PIREP mandated an examination of the four adjacent CIP grid points. To cover the same area for evaluating the GDCP each PIREP requires an examination of 64 GDCP cloud phase pixels. These spatially-devolved GDCP grid points then became the basis of comparison to the PIREPs.

For the GDCP the SLW condensate phase is thresholded under the assumption that the presence of SLW equates to a potential for icing. For this evaluation eight thresholds were used: 8, 16, 24, 32, 40, 48, 56, and 64 pixels.

4.2 Data

The valid time period for this evaluation is the same as for the CIP — 01 October 2003 to 31 March 2004 with valid times of 1445 and 2045 UTC (the nearest match to 1500 and 2100 UTC). A total of 316 GDCP files were available for verification with each file representing a combination of GOES-10 and GOES-12 data sets that have been stitched together at longitude 99.5° W.

Because the cloud phase observation is only valid at cloud top, eight different methods were employed in an attempt to discover the best way to determine whether or not a PIREP was close enough to the defined cloud top height. Each method was assigned a flag value and are described in Table 5. This table shows the counts for the numbers of PIREPs located within certain distances of the GDCP Cloud Top Height (CTH) measurements. These different groups of observations are used to perform separate analyses on GDCP.

4.3 Results

The overall results are diagrammed in Figures 5 and 6. Figure 5 is an ROC diagram of CIP, AIRMET, and GDCP for Flag 1. As shown in Figures 2 and 3, CIP shows good skill with a large area under the ROC curve. The single AIRMET data point is located just below the CIP line. The GDCP (cloud phase) has positive area under the curve and thus, positive skill, but has less area than the CIP. Figure 6 shows results for an evaluation similar to that shown in Figure 5 but for Flag 2. The results are similar in that CIP and the

Table 5: Counts of numbers of observations used in the verification of GDCP.

FLAG	All PIREPs within ...	YES MOG	NO
1	+/- 1,000 ft of median CTH (All Cloudy pixels)	134	1620
2	+/- 3,000 ft of median CTH (All Cloudy pixels)	349	3936
3	+/- 1,000 ft of median CTH (All SLW pixels)	130	1059
4	+/- 3,000 ft of median CTH (All SLW pixels)	328	2790
5	+/- 1,000 ft of min/max CTH (All Cloudy pixels)	643	6244
6	+/- 3,000 ft of min/max CTH (All Cloudy pixels)	828	8229
7	+/- 1,000 ft of min/max CTH (All SLW pixels)	393	3300
8	+/- 3,000 ft of min/max CTH (All SLW pixels)	552	4827

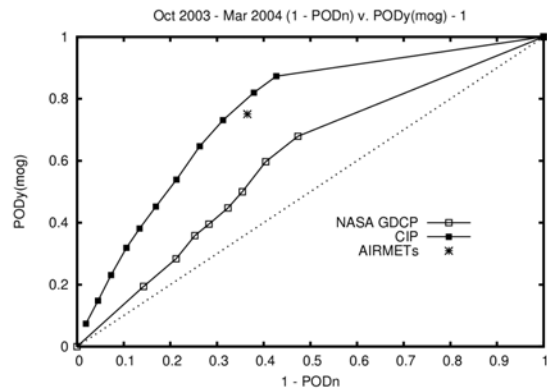


Figure 5: Comparison of PODy(MOG) vs. 1-PODn for CIP, AIRMETs, and GDCP using reports +/- 1,000 ft of the GDCP median CTH value for all cloudy pixels.

AIRMET show more skill than GDCP. In these two figures the PODy(MOG) values show that GDCP has some success in diagnosing the positive icing areas, assuming that the presence of SLW shows a potential for icing. The low PODn values are likely the reason for the poor skill of GDCP using all eight thresholds.

Table 6 shows the verification results using specific thresholds for both CIP (0.05 and 0.15) and GDCP for all flag values (see Table 5). These are compared with

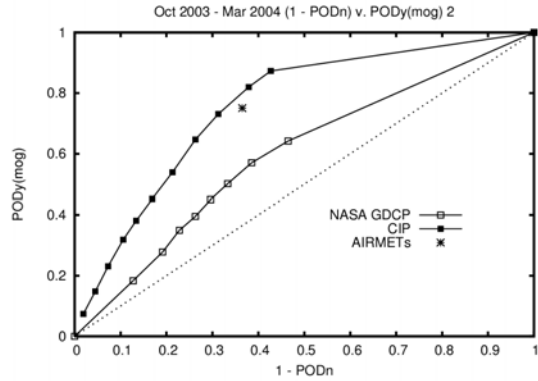


Figure 6: Comparison of $PODy(MOG)$ vs. $1-PODn$ for CIP, AIRMETs, and GDCP using reports $\pm 3,000$ ft of the GDCP median CTH value for all cloudy pixels.

the results for the AIRMETs. The results show that the $PODy(MOG)$ values for GDCP ranged from 0.578 to 0.822 and were somewhat comparable to the CIP (0.744 and 0.828) and the AIRMETs (0.751). The $PODn$ results are not as remarkable as the $PODy(MOG)$ results with scores ranging from 0.195 to 0.536 versus CIP (0.604 and 0.671) and the AIRMETs (0.635). The low $PODn$ for GDCP scores are also responsible for bringing down the True Skill Statistics (TSSs), which ranges from 0.002 to 0.206 compared to CIP (0.432 and 0.415) and the AIRMETs (0.386). Overall, the evaluation using GDCP-1 and GDCP-2 (Table 6) shows the best results for the GDCP with TSSs of 0.178 and 0.206 respectively.

The poor results for the GDCP for $PODn$ can be attributed to the nature of the product and the verification methods. Since the GDCP product is two-dimensional and is only valid near cloud-top, a smaller set of observations was used for verification. The area that was verified contained SLW and an assumption of positive icing potential was made in order to obtain a verifiable field. The problem with this assumption is that the presence of SLW does not necessarily imply that the area has icing. In the case where SLW is present but icing is not, a negative report of icing was recorded as a miss. Another apparent problem with the verification method is the lack of an exact CTH measurement. If a median cloud-top height measurement is too high and there is a negative report of icing in an area just above the real cloud top containing SLW, then a miss is recorded.

With the verification limited only to the areas around the GDCP CTH measurement, the low values of $PODn$ are not surprising. After all, the GDCP only attempts to detect areas of positive SLW and thus positive icing potential. If clear areas are added to the verification (i.e. areas above the maximum CTH measurement) then the $PODn$ results would likely improve. However, addition of the negative icing areas would most likely have a negative effect on the $PODy(MOG)$ statistics.

Table 6: Statistics for CIP, AIRMETs, and GDCP at Specific Thresholds.

Product	$PODy(MOG)$	$PODn$	TSS
CIP (.05)	0.828	0.604	0.432
CIP (.15)	0.744	0.671	0.415
AIRMET	0.751	0.635	0.386
GDCP-1	0.679	0.527	0.206
GDCP-2	0.642	0.536	0.178
GDCP-3	0.708	0.294	0.002
GDCP-4	0.741	0.306	0.047
GDCP-5	0.579	0.481	0.060
GDCP-6	0.578	0.499	0.077
GDCP-7	0.822	0.195	0.017
GDCP-8	0.790	0.241	0.031

Another potential problem with this verification approach is the difficulty in evaluating a high-resolution observational product using a low-resolution verification data set (PIREPs in this case). While this can, in part, be compensated for by trying to combine many of the high-resolution data pixels into larger spatial blocks, this approach will necessarily reduce the $PODn$, as we have seen in this analysis.

4.4 Plans for Further Analyses

In addition to cloud phase, the GDCP include a number of additional products that may be of use in CIP and which will be verified as these studies progress. These products include icing risk, liquid water path, water drop radius, optical depth, cloud top pressure, and the cloud base and top heights. It is likely, however, that a different sort of verification will be needed to judge the effective-ness of some of these products; possibly using PIREP reported icing intensity and/or research aircraft data.

In addition to the PIREP-based verification, we also plan to conduct a direct comparison of CIP and selected GDCP outputs including the total areas covered as well as overlapping and non-overlapping areas. In addition, we hope to derive statistics such as efficiency (POD divided by total area) to help us determine how the GDCP can best be incorporated into CIP.

5. SUMMARY

Although encouraging, the methods and results presented here should be considered preliminary. CIP already does an excellent job at diagnosing the potential for icing on a 20-km scale, but we hope to do better. Our plans for this product include the depiction of icing severity, better information on locations of supercooled large droplets (SLD), and higher resolution products for the terminal area. We have only modest skill to date on severity and SLD and hope that the advanced satellite products will help increase our skill. For the terminal area, resolution of 5 km, or smaller, and time scales of 15-30 min or shorter are needed, and these cannot be accomplished without satellite support. We already know, in a qualitative manner, the value of the advanced satellite products through our experience using them in field project forecasting exercises and it is now time to quantify their accuracy.

We know have available a number of unique sets of observations that should enable us to determine which advanced satellite products are the best for incorporation into CIP. We seek increased efficiency (greatest icing detection with smallest overwarning) and an improved icing severity algorithm. We also expect that the advanced satellite cloud products will enable more accurate icing diagnosis in areas where surface data are sparse, for example, over oceans and Alaska.

6. ACKNOWLEDGEMENTS

This work was supported by the NASA ASAP in conjunction with the FAA Aviation Weather Research Program. We would especially like to thank Anne Holmes for her expertise is working with large data files and complex verification procedures. Portions of this research are in response to requirements and funding by the Federal Aviation Administration (FAA). The views expressed are those of the authors and do not necessarily represent the official policy or position of the FAA.

7. REFERENCES

- Bernstein, B.C., F. McDonough, M.K. Politovich, B.G. Brown, T.P. Ratvasky, D.R. Miller, C.A. Wolff and G. Cuning, 2004: Current icing potential (CIP): Algorithm description and comparison with aircraft observations. Submitted to *J. Appl. Meteor.*
- Brown, B.G., 1996: Verification of in-flight icing forecasts: Methods and issues. Proceedings, FAA International Conference on Aircraft In-flight Icing, Report No. DOT/FAA/AR-96/81, II, 319-330.
- Brown, B.G., G. Thompson, R.T. Bruintjes, R. Bullock, and T. Kane, 1997: Intercomparison of in-flight icing algorithms. Part II: Statistical Verification results. *Weather and Forecasting*, **12**, 890-914.
- Brown, B.G., T.L. Kane, R. Bullock, and M.K. Politovich, 1999: Evidence of improvements in the quality of in-flight icing algorithms. *Proceedings, 8th Conference on Aviation, Range, and Aerospace Meteorology*, Dallas, TX, 10-15 January, American Meteorological Society (Boston), 48-52.
- Dong, X., P. Minnis, G. G. Mace, W. L. Smith, Jr., M. Poellot, R. T. Marchand, and A. D. Rapp, 2002: Comparison of stratus cloud properties deduced from surface, GOES, and aircraft data during the March 2000 ARM Cloud IOP. *J. Atmos. Sci.*, **59**, 3256-3284.
- Minnis, P., D. P. Garber, D. F. Young, R. F. Arduini, and Y. Takano, 1998: Parameterization of reflectance and effective emittance for satellite remote sensing of cloud properties. *J. Atmos. Sci.*, **55**, 3313-3339.
- Minnis, P., D. P. Kratz, J. A. Coakley, Jr., M. D. King, D. Garber, P. Heck, S. Mayor, D. F. Young, and R. Arduini, 1995: Cloud Optical Property Retrieval (Subsystem 4.3). "Clouds and the Earth's Radiant Energy System (CERES) Algorithm Theoretical Basis Document, Volume III: Cloud Analyses and Radiance Inversions (Subsystem 4)", NASA RP 1376 Vol. 3, edited by CERES Science Team, pp. 135-176.
- Minnis, P., W. L. Smith, Jr., L. Nguyen, J. J. Murray, P. W. Heck, and M. M. Khaiyer, 2003: Near-real-time satellite cloud products for icing detection and aviation weather over the USA. *Proc. FAA In-Flight Icing/De-icing International Conference*, Chicago, IL, June 16-20, CD_ROM, 2003-01-2097.
- Minnis, P., W. L. Smith, Jr., L. Nguyen, M. M. Khaiyer, D. A. Spangenberg, P. W. Heck, R. Palikonda, B. C. Bernstein, and F. McDonough, 2004: A real-time satellite-based icing detection system. *Proc. 14th Intl. Conf Clouds and Precip.- ICCP 2004*, Bologna, Italy, July 18-23.
- Minnis, P., W. L. Smith, Jr., D. F. Young, L. Nguyen, A. D. Rapp, P. W. Heck, S. Sun-Mack, Q. Treppe, and Y. Chen, 2001: A near-real time method for deriving cloud and radiation properties from satellites for weather and climate studies. *Proc. AMS 11th Conf. Satellite Meteorology and Oceanography*, Madison, WI, Oct. 15-18, 477-480.
- McDonough, F. and B.C. Bernstein, 1999: Combining satellite, radar and surface observations with model data to create a better aircraft icing diagnosis. *Proceedings, 8th Conference on Aviation, Range and Aerospace Meteorology*, Dallas, 10-15 January. Amer. Meteor. Soc., Boston, 467-471.
- Smith, W. L., Jr., P. Minnis, B. C. Bernstein, F. McDonough, and M. M. Khaiyer, 2003: Comparison of supercooled liquid water cloud properties derived from satellite and aircraft measurements. *Proc. FAA In-Flight Icing/De-icing International Conference*, Chicago, IL, June 16-20, CD_ROM, 2003-01-2156.
- Smith, W. L., Jr., P. Minnis, B. C. Bernstein, A. D. Rapp, and P. W. Heck, 2002: Supercooled liquid water cloud properties derived from GOES: Comparisons

with in situ aircraft measurements. *10th AMS Conf. Aviation, Range, and Aerospace Meteorol.*, Portland, OR, May 13-16, 89-92.

Smith, W. L., Jr., P. Minnis, and D. F. Young, 2000: An icing product derived from operational satellite data. *Proc. AMS 9th Conf. Aviation, Range, and Aerospace Meteorol.*, Orlando, FL, 11-15 Sept., 256-259.

Trepte, Q., Y. Chen, S. Sun-Mack, P. Minnis, D. F. Young, B. A. Baum, and P. W. Heck, 1999: Scene identification for the CERES cloud analysis subsystem. *Proc. AMS 10th Conf. Atmos. Rad.*, Madison, WI, June 28 – July 2, 169-172.